Supplement of Biogeosciences, 19, 1395–1420, 2022
https://doi.org/10.5194/bg-19-1395-2022-supplement


Biogeosciences Open Access EGU

*Supplement of*

# Bacterial and eukaryotic intact polar lipids point to in situ production as a key source of labile organic matter in hadal surface sediment of the Atacama Trench

**Edgart Flores et al.**

*Correspondence to:* Edgart Flores (edgart.flores@imo-chile.cl) and Julio Sepúlveda (jsepulveda@colorado.edu)

**SUPPLEMENTARY MATERIAL**

Flores et al. 'Bacterial and eukaryotic intact polar lipids point to in situ production as a key source of labile organic matter in hadal surface sediment of the Atacama Trench'

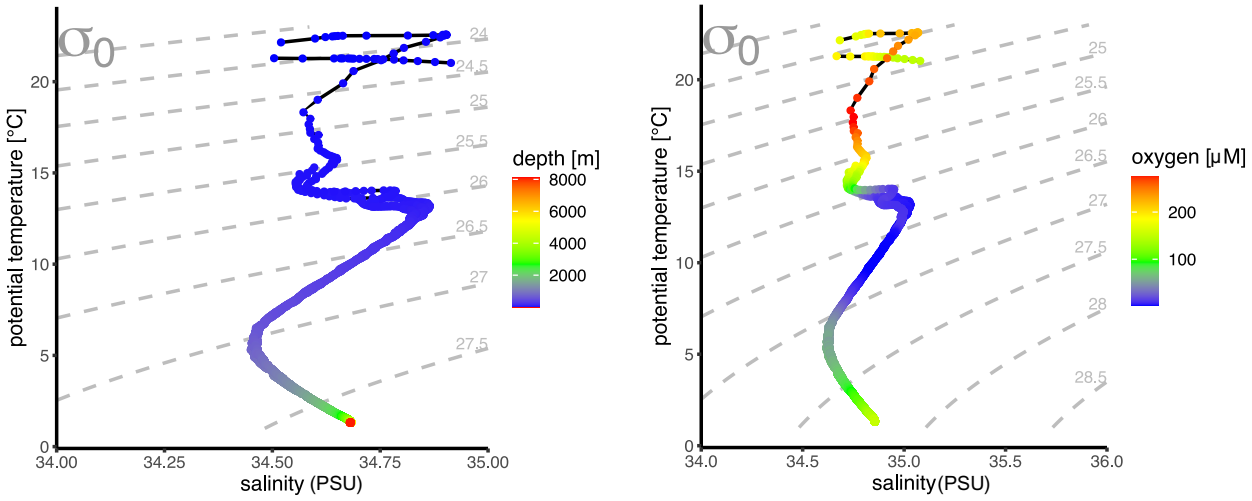


**Figure S1**. The potential temperature−salinity (θ−s) diagrams from CTD data coupled to an AUV (autonomous underwater vehicle). The color scale is related to depth (m) and oxygen concentration (µM).

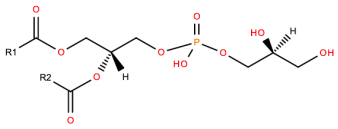

Phosphatidylglycerol Head group (PG)

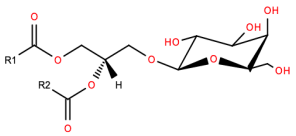

Monogalactosyl diacylglycerol Head group (MGDG)

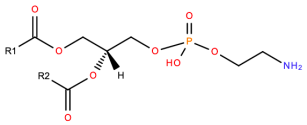

Phosphatidylethanolamine Head group (PE)

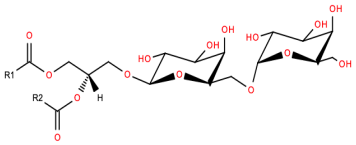

Digalactosyl diacylglycerol Head group (DGDG)

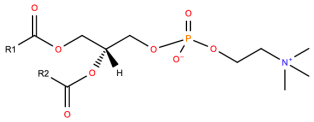

Phosphatidylcholine Head group (PC)

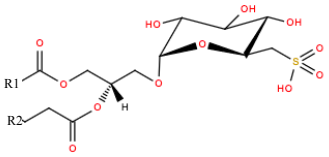

Sulfoquinovosyl diacylglycerol Head group (SQDG)

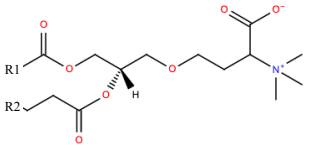

Diacylglyceryltrimethylhomoserine
Head group (DGTS)

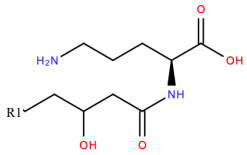

Ornithine lipid Head group (OL)

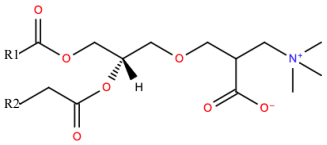

Diacylglyceryl-hydroxymethyltrimethyl-β-alanine
Head group (DGTA)

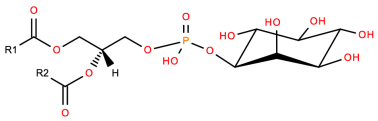

Phosphatidylinositol Head group (PI)

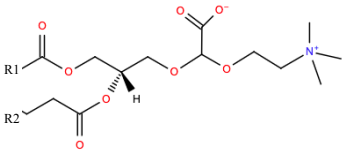

Diacylglyceryl carboxyhydroxymethylcholine
Head group (DGCC)

**Figure S2.** IPL chemical structures from the LIPID MAPS database (Sud et al., 2007). R1 and R2 represent acyl groups, whereas the charges are those expected at seawater pH.


**Figure S3.** Relative abundances of IPLs distinctive (red color; Cantarero et al. 2020) and non-distinctive (turquoise; total IPLs minus IPLs from Chlorophyll maximum) of the Chlorophyll maximum for all samples.

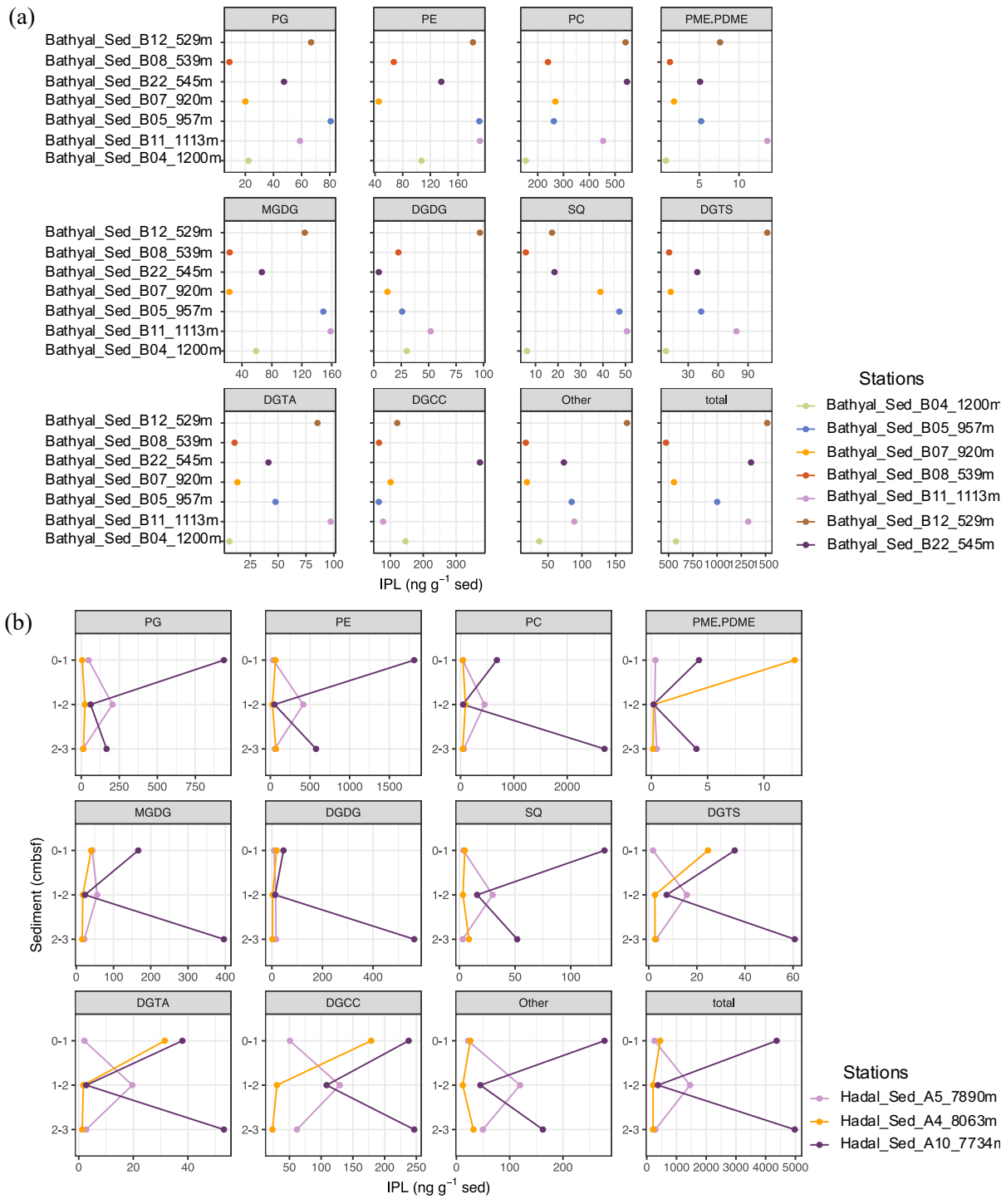


**Figure S4.** Total concentration of IPL by class, in (a) bathyal and (b) hadal sediment samples.

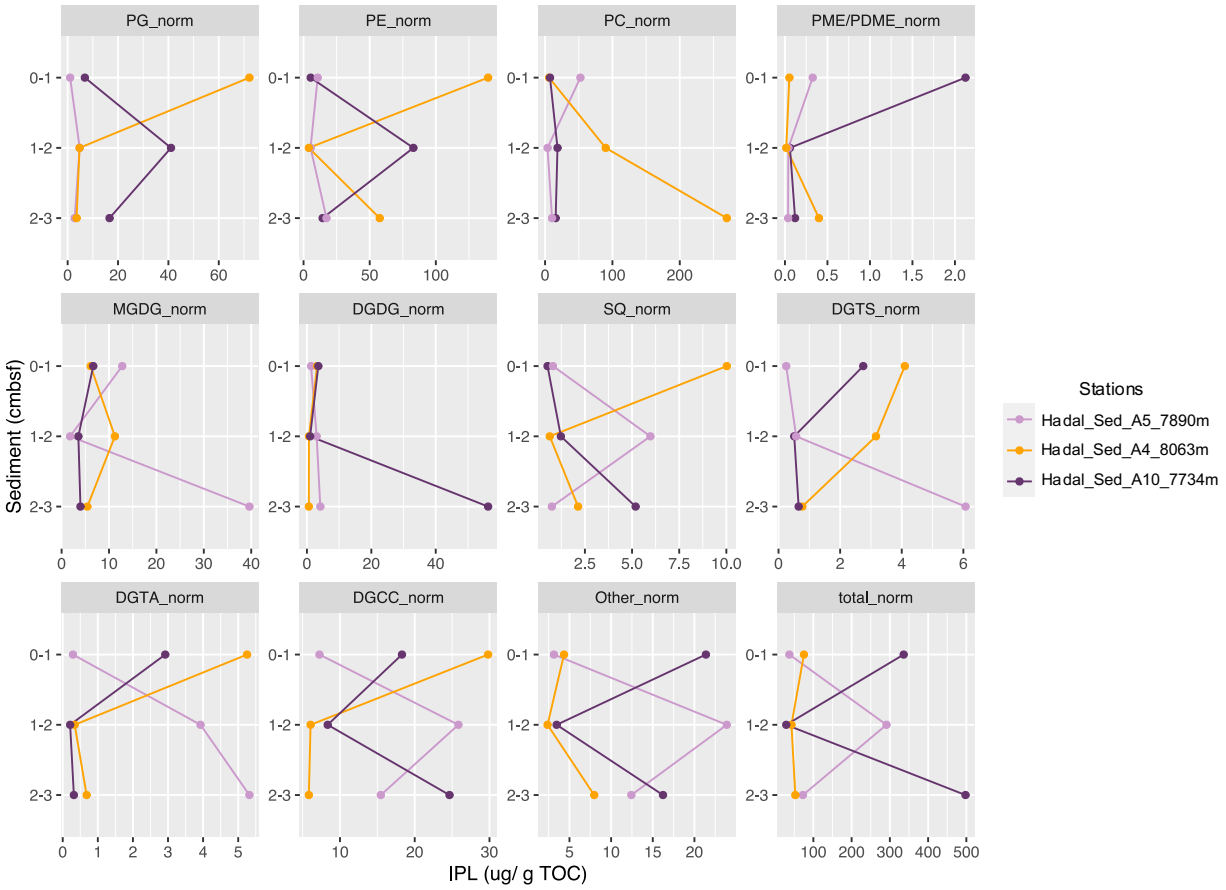


**Figure S5.** TOC-normalized IPL concentration (μg IPL/g TOC) in hadal sediments.

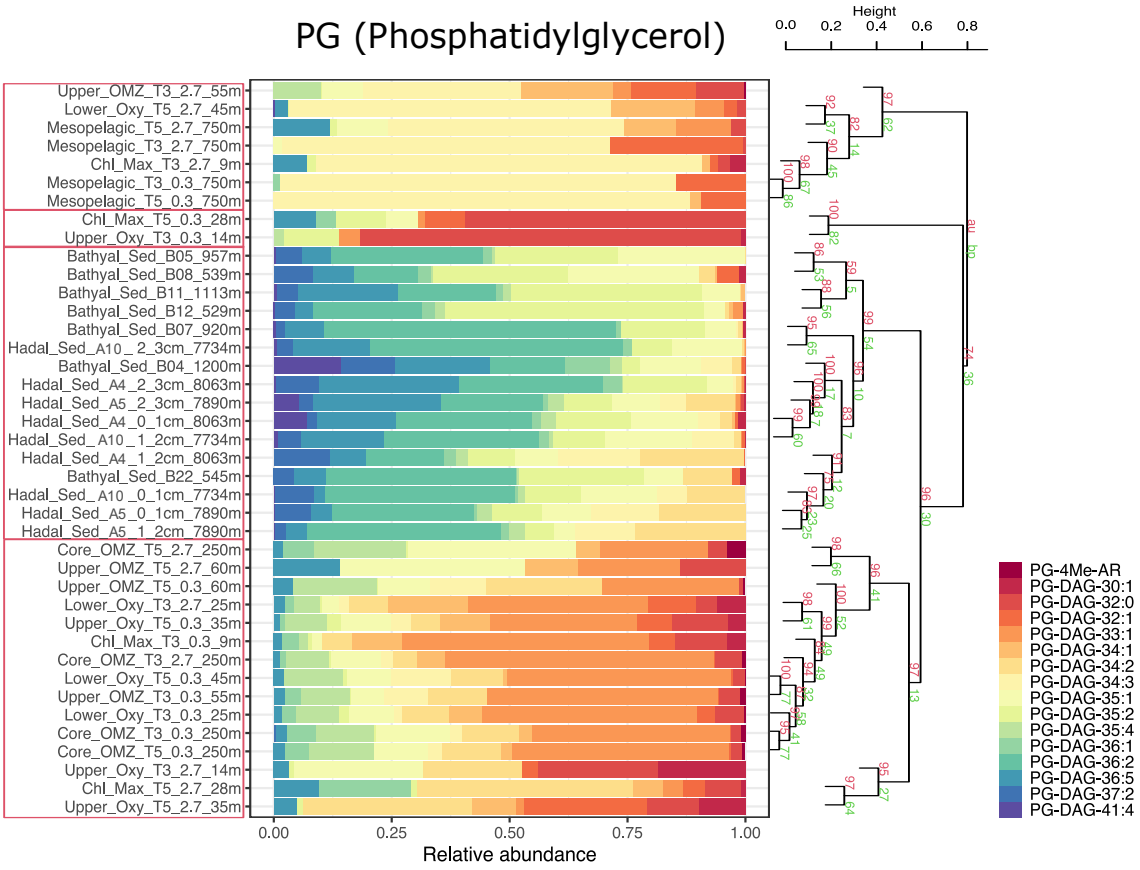


**Figure S6.** Cumulative bar chart of PG phospholipid fractional abundances. The number of carbon atoms and unsaturation in core fatty acids follows the order shown in the legend. The right panel depicts a cluster analysis with AU and BP shown in red and green, respectively, and p-values shown at branching points. The number of bootstrap replicates is 10000. Clusters with AU ≥ 95% confidence are highlighted in red boxes on the left-hand side.

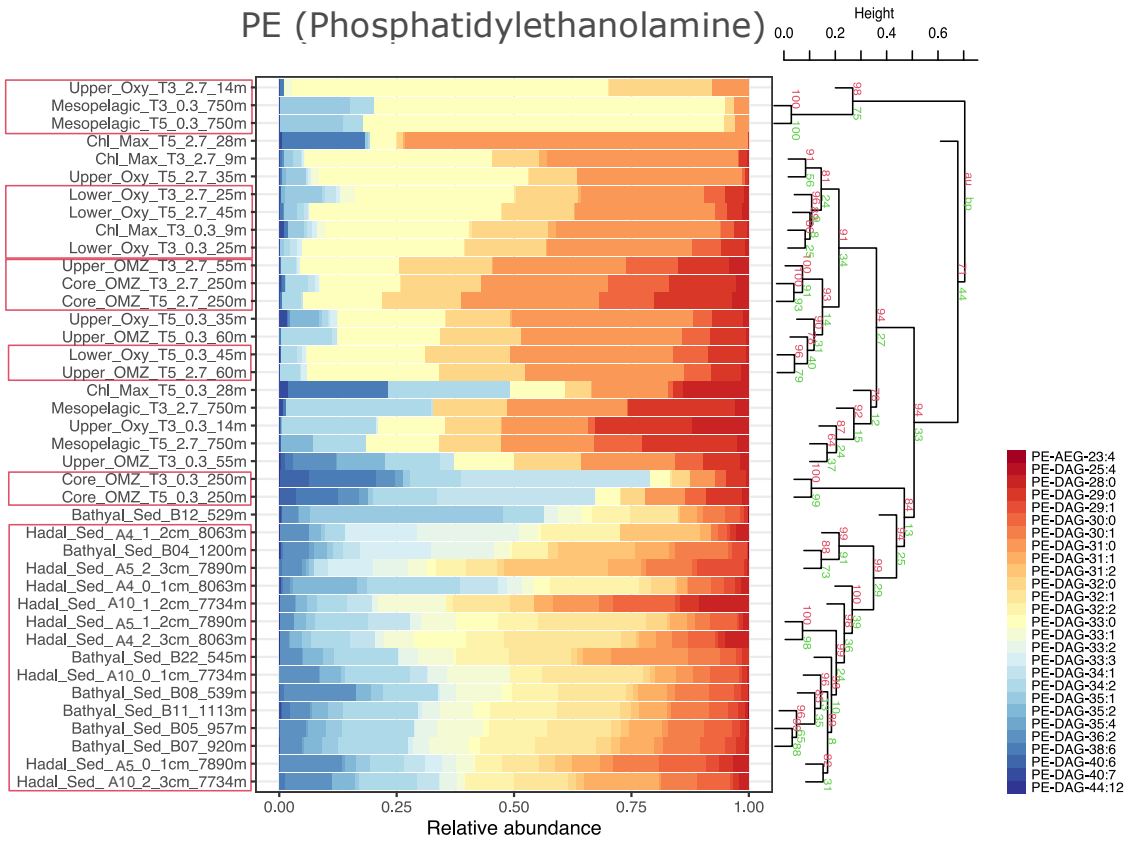


**Figure S7.** Cumulative bar chart of PE phospholipid fractional abundances. The number of carbon atoms and unsaturation in core fatty acids follows the order shown in the legend. The right panel depicts a cluster analysis with AU and BP shown in red and green, respectively, and p-values shown at branching points. The number of bootstrap replicates is 10000. Clusters with AU ≥ 95% confidence are highlighted in red boxes on the left-hand side.

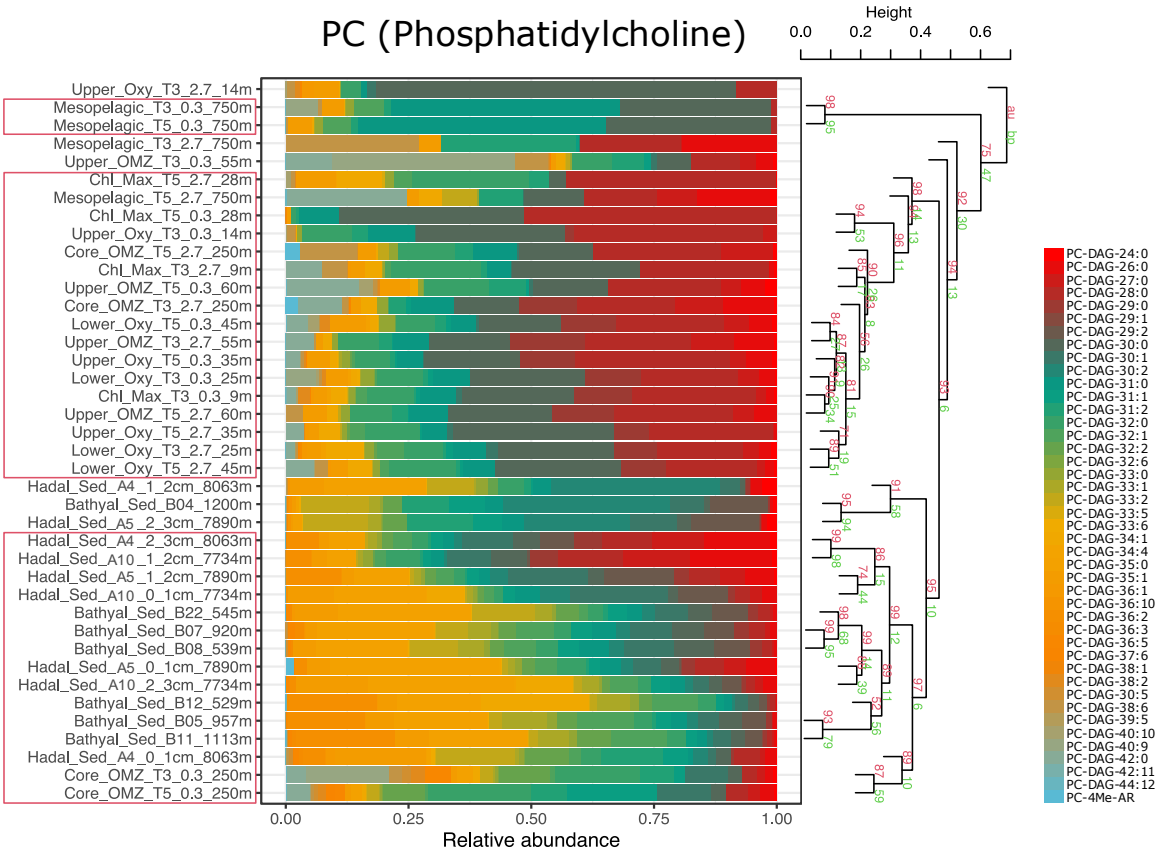


**Figure S8.** Cumulative bar chart of PC phospholipid fractional abundances. The number of carbon atoms and unsaturation in core fatty acids follows the order shown in the legend. The right panel depicts a cluster analysis with AU and BP shown in red and green, respectively, and p-values shown at branching points. The number of bootstrap replicates is 10000. Clusters with AU ≥ 95% confidence are highlighted in red boxes on the left-hand side.

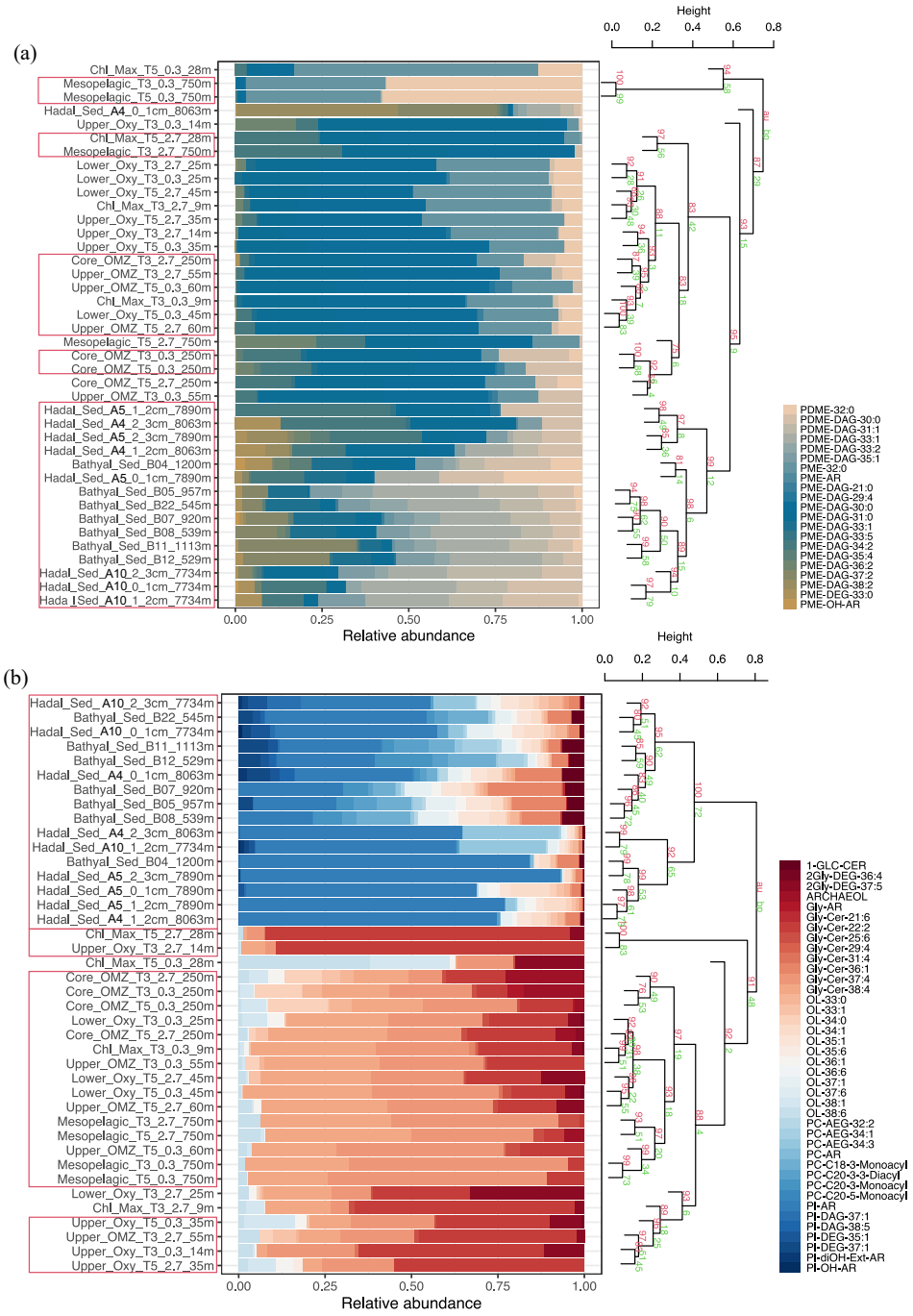


**Figure S9.** Cumulative bar chart of IPLs fractional abundances. a) PDME, PME; b) Other lipids. The number of carbon atoms and unsaturation in core fatty acids follows the order shown in the legend. The right panel depicts a cluster analysis with approximately unbiased (AU) and bootstrap probability (BP) shown in red and green, respectively, and p-values shown at branching points. The number of bootstrap replicates is 10000. Clusters with AU ≥ 95% confidence are highlighted in red boxes on the left-hand side.

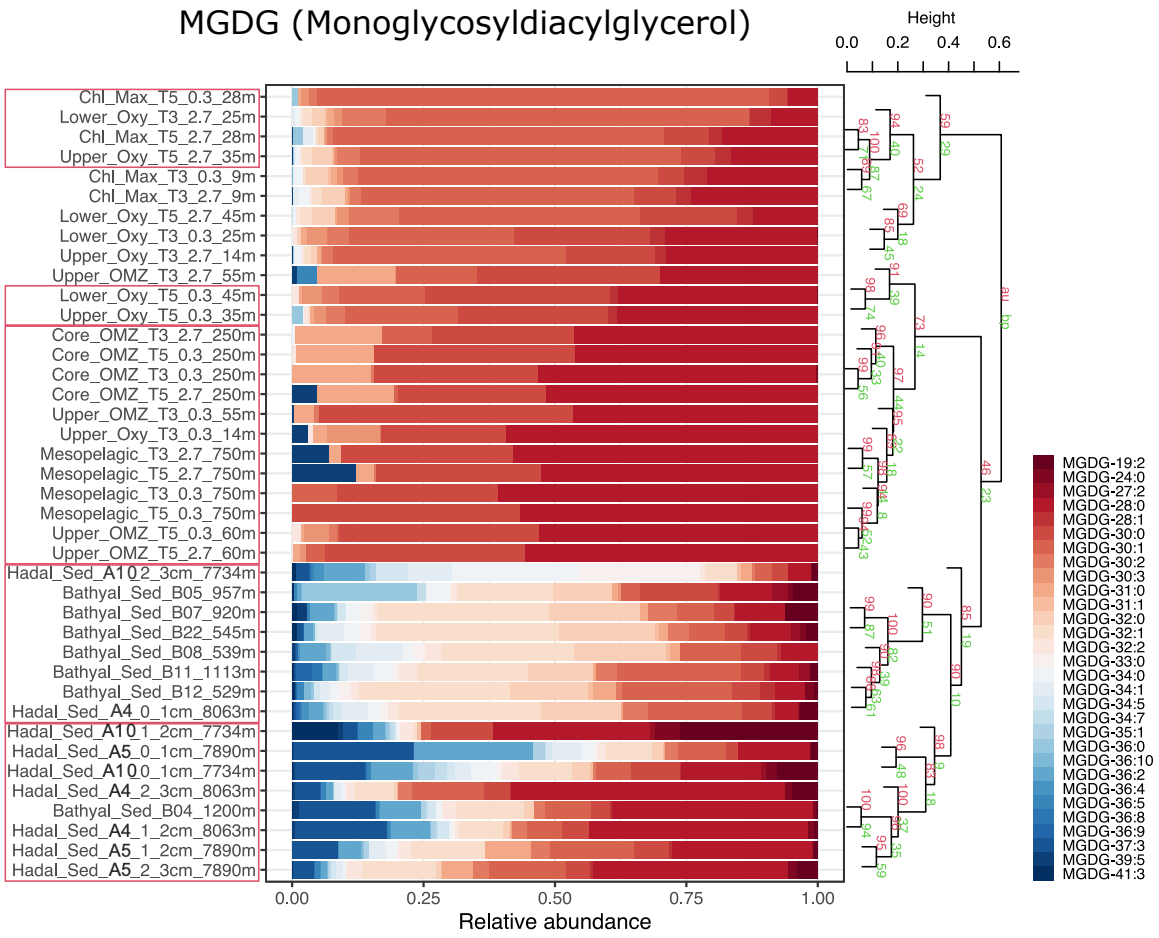


**Figure S10.** Cumulative bar chart of MGDG glycolipid fractional abundances. The number of carbon atoms and unsaturation in core fatty acids follows the order shown in the legend. The right panel depicts a cluster analysis with AU and BP in red and green, respectively, and p-values shown at branching points. The number of bootstrap replicates is 10000. Clusters with AU ≥ 95% confidence are highlighted in red boxes on the left-hand side.

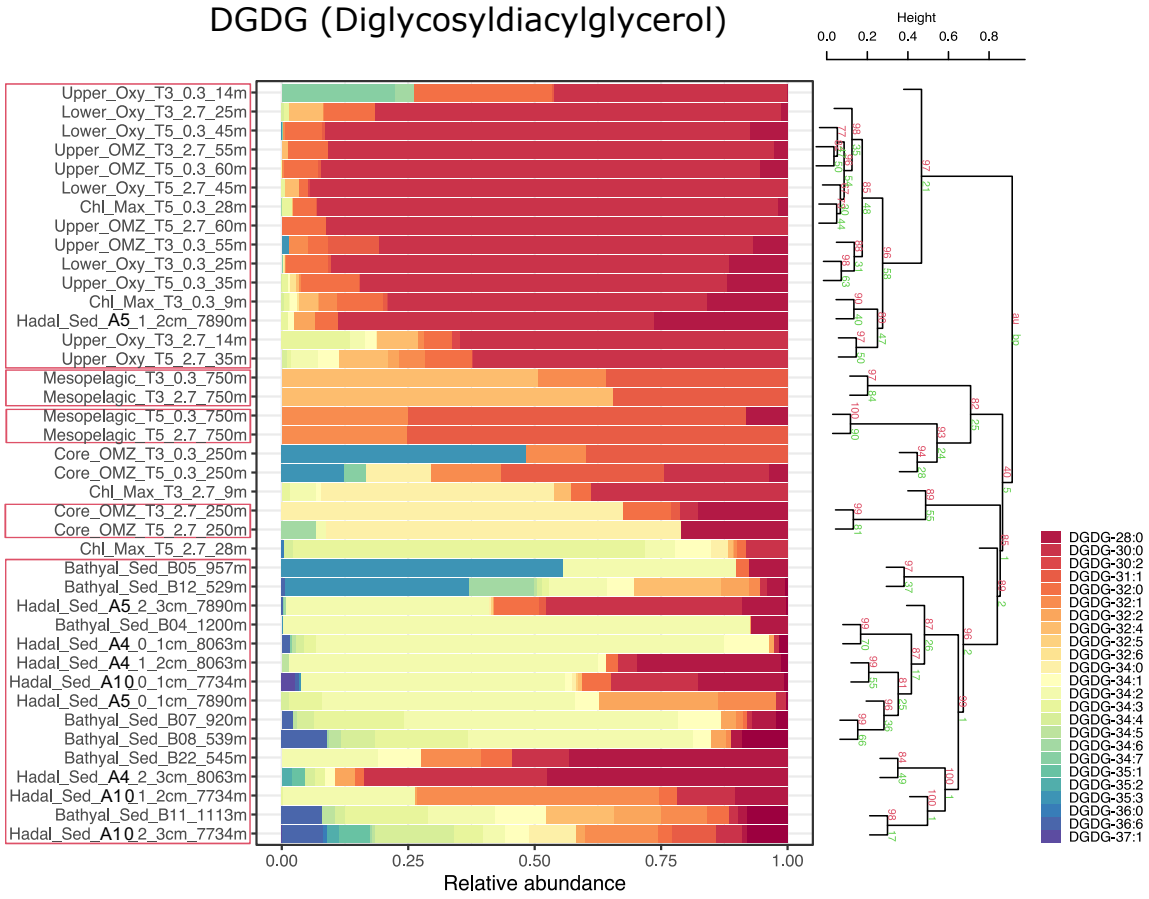


**Figure S11.** Cumulative bar chart of DGDG glycolipid fractional abundances. The number of carbon atoms and unsaturation in core fatty acids follows the order shown in the legend. The right panel depicts a cluster analysis with AU and BP in red and green, respectively, and p-values shown at branching points. The number of bootstrap replicates is 10000. Clusters with AU ≥ 95% confidence are highlighted in red boxes on the left-hand side.

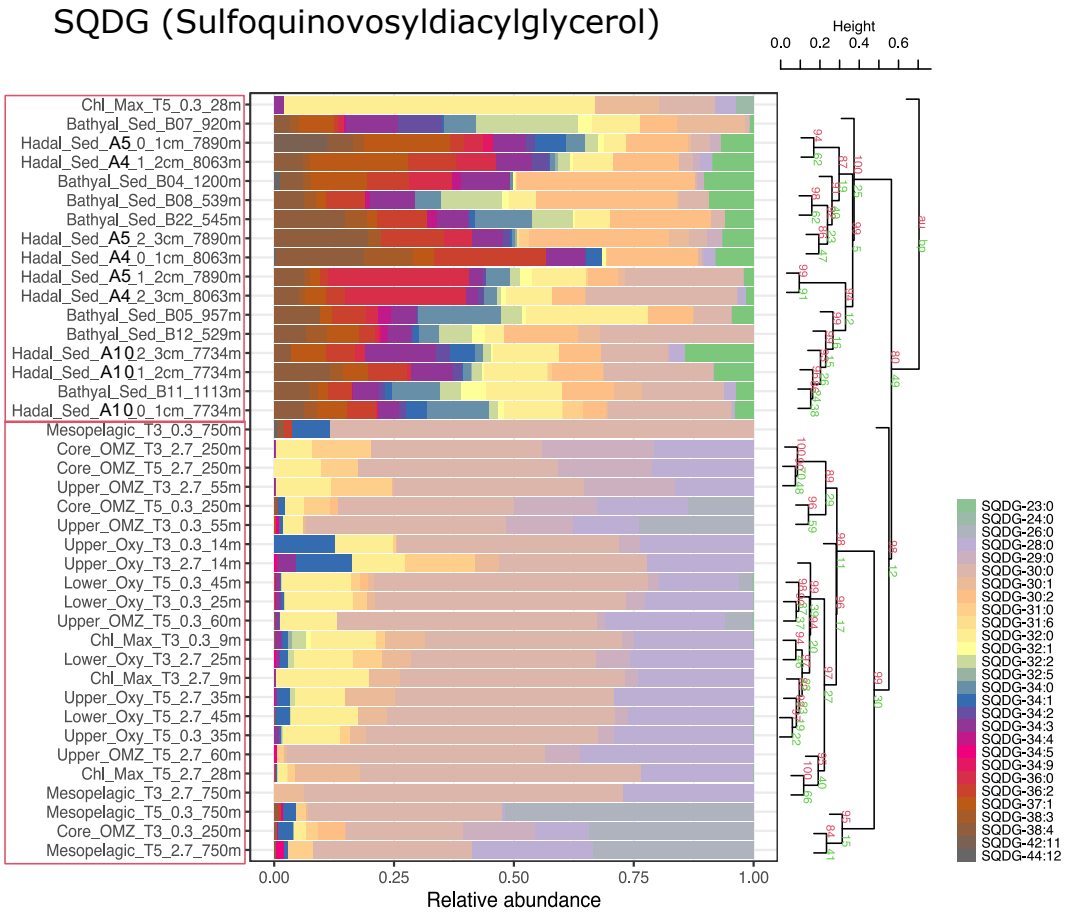


**Figure S12**. Cumulative bar chart of SGDG glycolipid fractional abundances. The number of carbon atoms and unsaturation in core fatty acids follows the order shown in the legend. The right panel depicts a cluster analysis with AU and BP in red and green, respectively, and p-values shown at branching points. The number of bootstrap replicates is 10000. Clusters with AU ≥ 95% confidence are highlighted in red boxes on the left-hand side.

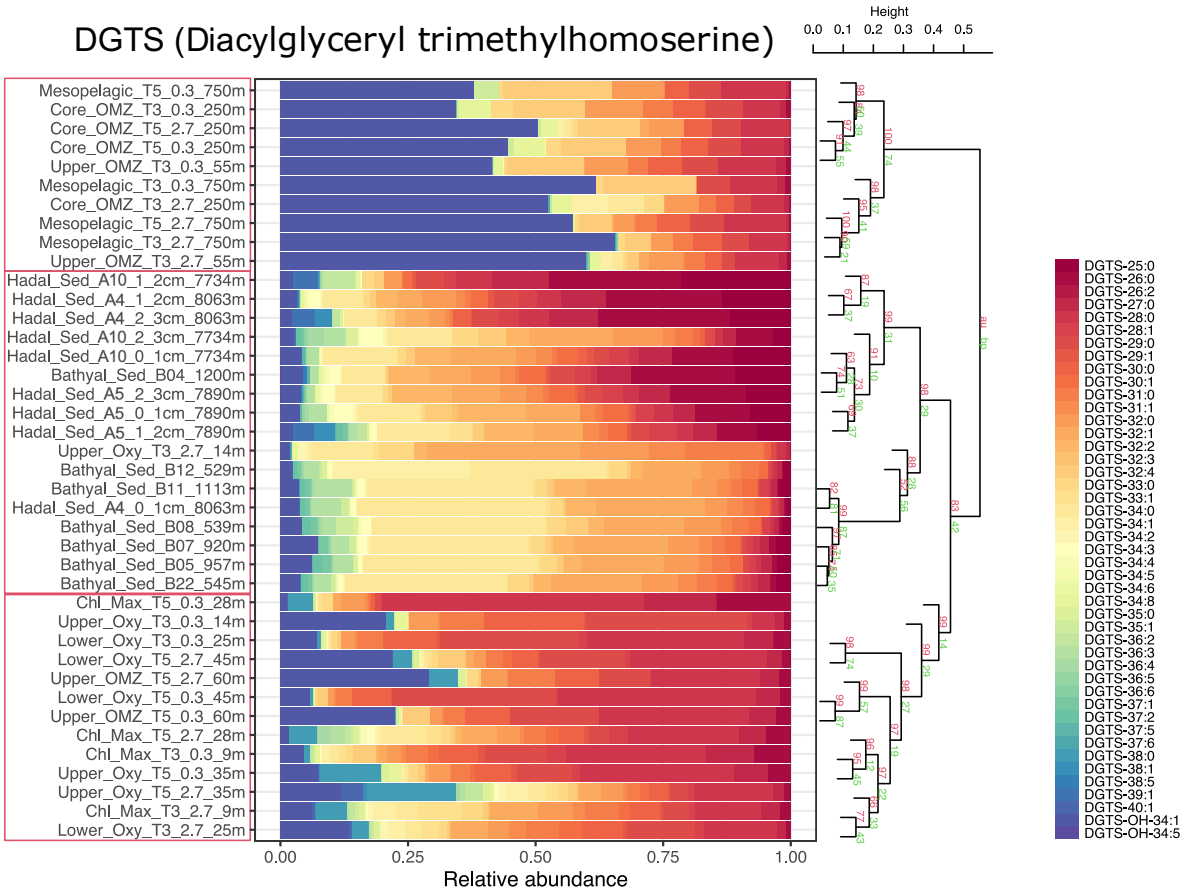


**Figure S13.** Cumulative bar chart of DGTS betaine fractional abundances. The number of carbon atoms and unsaturation in core fatty acids follows the order shown in the legend. The right panel depicts a cluster analysis with AU and BP in red and green, respectively, and p-values shown at branching points. The number of bootstrap replicates is 10000. Clusters with AU $\geq$ 95% confidence are highlighted in red boxes on the left-hand side.

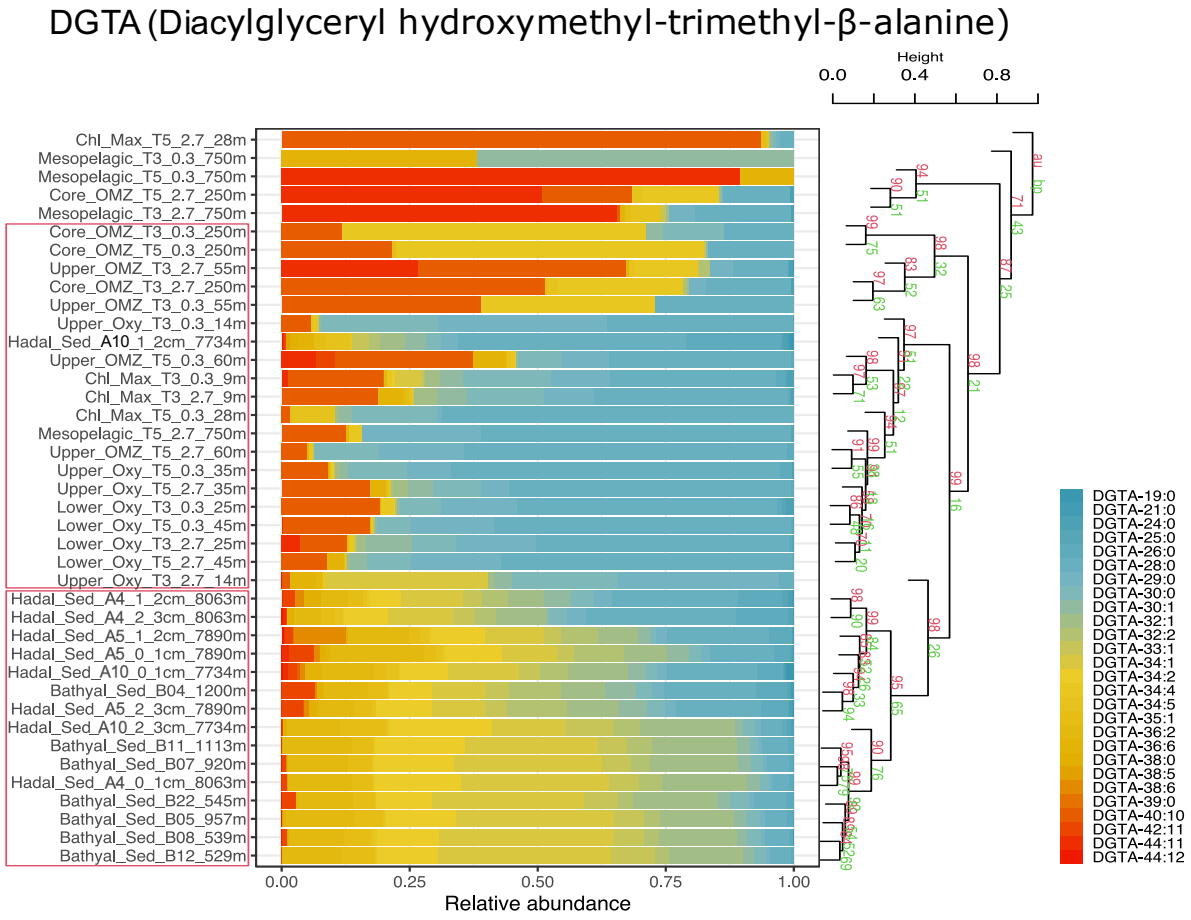


**Figure S14.** Cumulative bar chart of DGTA betaine fractional abundances. The number of carbon atoms and unsaturation in core fatty acids follows the order shown in the legend. The right panel depicts a cluster analysis with AU and BP in red and green, respectively, and p-values shown at branching points. The number of bootstrap replicates is 10000. Clusters with AU ≥ 95% confidence are highlighted in red boxes on the left-hand side.

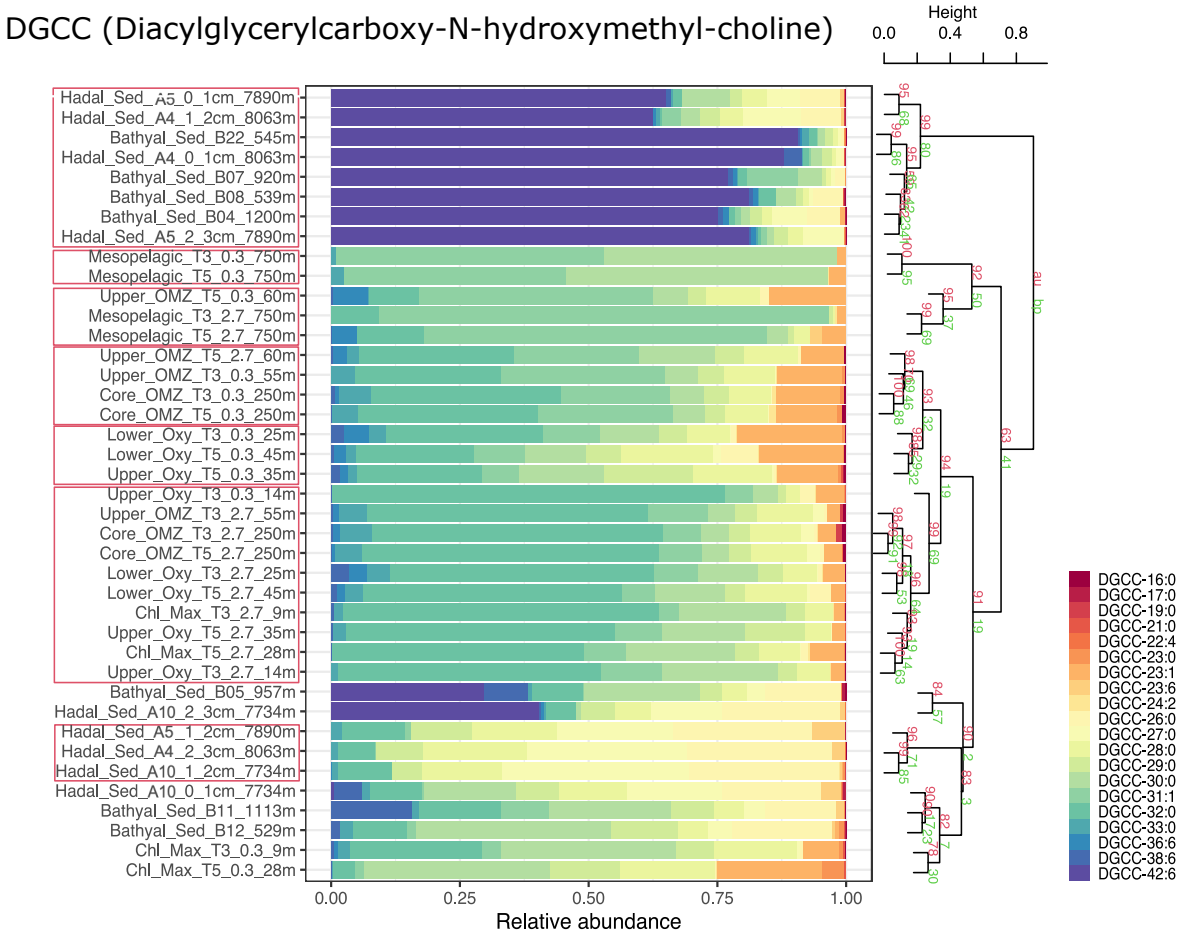


**Figure S15**. Cumulative bar chart of DGCC betaine fractional abundances. The number of carbon atoms and unsaturation in core fatty acids follows the order shown in the legend. The right panel depicts a cluster analysis with AU and BP in red and green, respectively, and p-values shown at branching points. The number of bootstrap replicates is 10000. Clusters with AU ≥ 95% confidence are highlighted in red boxes on the left-hand side.

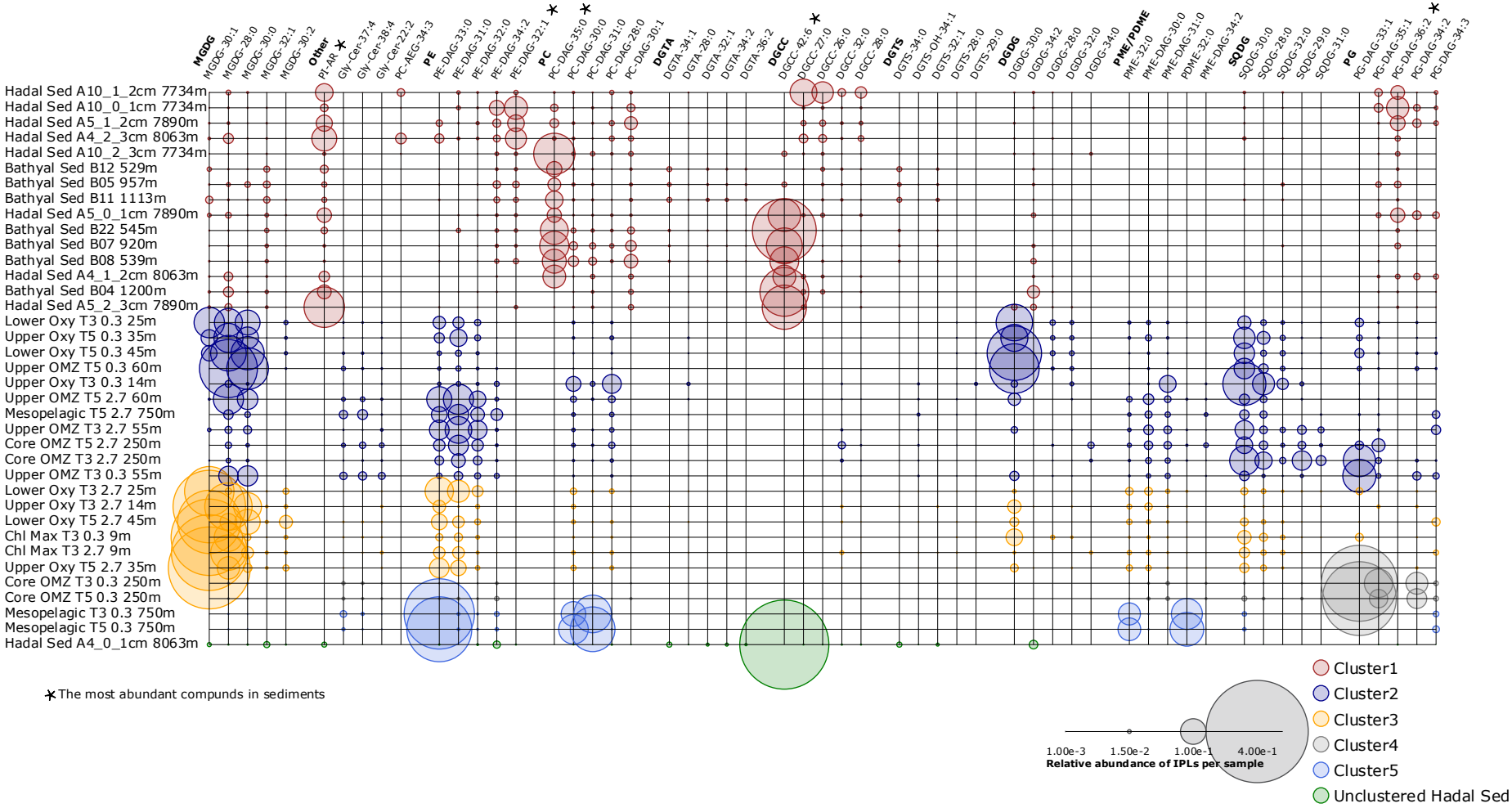


**Figure S16.** Relative abundance of the five most abundant IPL compounds per class in our study. Circle size is proportional to the relative abundance of IPL compounds per sample. Samples are organized along the Y axis and shown in colors that match the hierarchical cluster analysis in Fig. 8. The legend shows the scale for circumference size.

**Table S1.** Similarity percentage (SIMPER) analysis showing the average abundance and contribution of IPLs that explained the main differences among the hierarchical clusters in Fig. 8, and that include the water column and sediment samples.

| Groups Cluster 1 & Cluster 2<br>Average dissimilarity = 85.46 | | | | | | |
|---|---|---|---|---|---|---|
| IPLs | Average Cluster 1 | Average Cluster 2 | Average dissimilarity | Dissimilarity/SD | Contribution (%) | Cumulative (%) |
| DGCC-42:6 | 0.07 | 0 | 3.74 | 0.9 | 4.37 | 4.37 |
| SQDG-30:0 | 0 | 0.08 | 3.6 | 1.93 | 4.21 | 8.59 |
| DGDG-30:0 | 0 | 0.07 | 3.52 | 0.95 | 4.12 | 12.71 |
| MGDG-28:0 | 0.02 | 0.08 | 3.48 | 1.13 | 4.08 | 16.79 |
| MGDG-30:0 | 0 | 0.07 | 3.06 | 1.23 | 3.58 | 20.37 |
| PC-DAG-35:0 | 0.06 | 0 | 2.96 | 1.3 | 3.46 | 23.83 |
| PE-DAG-31:0 | 0.01 | 0.06 | 2.64 | 1.59 | 3.09 | 26.92 |
| PI-AR | 0.05 | 0 | 2.32 | 1.2 | 2.72 | 29.64 |
| PE-DAG-33:0 | 0.01 | 0.04 | 1.93 | 1.47 | 2.25 | 31.89 |
| SQDG-28:0 | 0 | 0.04 | 1.89 | 1.81 | 2.21 | 34.1 |
| PG-DAG-33:1 | 0 | 0.04 | 1.87 | 0.85 | 2.19 | 36.3 |
| PE-DAG-32:0 | 0 | 0.03 | 1.5 | 1.42 | 1.76 | 38.05 |
| PG-DAG-36:2 | 0.03 | 0 | 1.37 | 1.15 | 1.6 | 39.65 |
| PE-DAG-32:1 | 0.03 | 0 | 1.31 | 0.95 | 1.53 | 41.19 |
| MGDG-30:1 | 0.01 | 0.02 | 1.26 | 0.76 | 1.48 | 42.66 |
| PC-DAG-30:2 | 0.02 | 0 | 1.24 | 0.62 | 1.45 | 44.11 |
| PC-DAG-30:1 | 0.02 | 0 | 1.17 | 1.67 | 1.37 | 45.48 |
| PE-DAG-29:0 | 0 | 0.03 | 1.15 | 1.06 | 1.35 | 46.83 |
| PME-DAG-30:0 | 0 | 0.02 | 1.1 | 1.89 | 1.29 | 48.12 |
| PME-DAG-31:0 | 0 | 0.02 | 1.09 | 1.32 | 1.28 | 49.39 |
| PC-DAG-29:2 | 0.02 | 0 | 0.95 | 1.4 | 1.11 | 50.51 |
| Groups Cluster 1 & Cluster 3<br>Average dissimilarity = 84.70 | | | | | | |
| IPLs | Average Cluster 1 | Average Cluster 3 | Average dissimilarity | Dissimilarity/SD | Contribution (%) | Cumulative (%) |
| MGDG-30:1 | 0.01 | 0.27 | 13.24 | 6.19 | 15.63 | 15.63 |
| MGDG-28:0 | 0.02 | 0.1 | 4.35 | 1.68 | 5.14 | 20.77 |
| DGCC-42:6 | 0.07 | 0 | 3.74 | 0.9 | 4.41 | 25.19 |
| PC-DAG-35:0 | 0.06 | 0 | 2.95 | 1.29 | 3.49 | 28.67 |
| PE-DAG-33:0 | 0.01 | 0.06 | 2.83 | 2.01 | 3.34 | 32.01 |
| MGDG-30:0 | 0 | 0.05 | 2.44 | 1.3 | 2.88 | 34.89 |
| PI-AR | 0.05 | 0 | 2.32 | 1.2 | 2.74 | 37.63 |
| PE-DAG-31:0 | 0.01 | 0.05 | 2.07 | 1.73 | 2.44 | 40.07 |
| DGDG-30:0 | 0 | 0.03 | 1.6 | 1.64 | 1.89 | 41.97 |
| SQDG-30:0 | 0 | 0.03 | 1.45 | 2.05 | 1.72 | 43.68 |
| PG-DAG-36:2 | 0.03 | 0 | 1.37 | 1.14 | 1.61 | 45.3 |
| PE-DAG-32:1 | 0.03 | 0 | 1.29 | 0.94 | 1.53 | 46.82 |
| PC-DAG-30:2 | 0.02 | 0 | 1.24 | 0.62 | 1.46 | 48.29 |
| PC-DAG-30:1 | 0.02 | 0 | 1.15 | 1.63 | 1.36 | 49.64 |
| MGDG-30:2 | 0 | 0.02 | 1.08 | 1.6 | 1.27 | 50.92 |
| Groups Cluster 1 & Cluster 4<br>Average dissimilarity = 85.99 | | | | | | |
| IPLs | Average Cluster 1 | Average Cluster 4 | Average dissimilarity | Dissimilarity/SD | Contribution (%) | Cumulative (%) |
| PG-DAG-33:1 | 0 | 0.29 | 14.63 | 66.25 | 17.02 | 17.02 |
| PG-DAG-35:4 | 0 | 0.09 | 4.24 | 36.43 | 4.93 | 21.95 |
| PG-DAG-35:1 | 0.01 | 0.09 | 4.05 | 3.59 | 4.71 | 26.67 |
| DGCC-42:6 | 0.07 | 0 | 3.74 | 0.89 | 4.35 | 31.01 |
| PG-DAG-34:2 | 0.01 | 0.08 | 3.63 | 5.35 | 4.22 | 35.23 |
| PC-DAG-35:0 | 0.06 | 0 | 2.89 | 1.26 | 3.36 | 38.6 |
| PI-AR | 0.05 | 0 | 2.32 | 1.18 | 2.7 | 41.3 |
| PG-DAG-36:1 | 0 | 0.04 | 1.8 | 6.37 | 2.09 | 43.39 |
| PE-DAG-34:1 | 0.01 | 0.04 | 1.75 | 4.39 | 2.03 | 45.42 |
| PG-DAG-36:2 | 0.03 | 0 | 1.37 | 1.13 | 1.59 | 47.01 |
| PE-DAG-32:1 | 0.03 | 0 | 1.3 | 0.93 | 1.51 | 48.52 |
| PC-DAG-30:2 | 0.02 | 0 | 1.24 | 0.61 | 1.44 | 49.96 |
| Groups Cluster 1 & Cluster 5<br>Average dissimilarity = 89.03 | | | | | | |
| IPLs | Average Cluster 1 | Average Cluster 5 | Average dissimilarity | Dissimilarity/SD | Contribution (%) | Cumulative (%) |
| PE-DAG-33:0 | 0.01 | 0.26 | 12.94 | 17.5 | 14.54 | 14.54 |
| PC-DAG-31:0 | 0.01 | 0.16 | 7.47 | 9.31 | 8.39 | 22.93 |
| PDME-32:0 | 0 | 0.13 | 6.33 | 22.82 | 7.11 | 30.03 |
| PC-DAG-30:0 | 0.01 | 0.11 | 4.66 | 6.45 | 5.24 | 35.27 |
| PME-32:0 | 0 | 0.09 | 4.37 | 68.49 | 4.91 | 40.18 |
| DGCC-42:6 | 0.07 | 0 | 3.74 | 0.89 | 4.2 | 44.38 |
| PC-DAG-35:0 | 0.06 | 0 | 2.96 | 1.28 | 3.33 | 47.71 |
| PI-AR | 0.05 | 0 | 2.32 | 1.18 | 2.61 | 50.31 |